BIOENGINEERED
2017, VOL. 8, NO. 1, 45–54
http://dx.doi.org/10.1080/21655979.2016.1227578

Taylor & Francis
Taylor & Francis Group

RESEARCH PAPER

Altered microRNA expression profiles in lung damage induced by nanosized SiO_2

Hong Yang, Yingjian Zhang, Wenchao Li, Canshan Lao, Mingyue Li, and Yi Zheng

Key Laboratory of Environmental Medicine Engineering, Ministry of Education, School of Public Health, Southeast University, Nanjing, China

ABSTRACT

The objective of the present research is to explore miRNAs expression profiles in lung tissue of rat treated by nanosized SiO_2 in the light of normal at diverse dosages, time, predict their target genes, and probe the biological function and regulation of miRNA in the lung damage process caused by nanosized SiO_2. Up-regulation of rno-miR-208, rno-miR-212 and rno-miR-18a in lung tissue mainly characterized by inflammation of SD rats caused by nanosized SiO_2 particles instilled intratracheally at 7^{th}, 15^{th} 30^{th} d using Illumina HiSeq2000 sequencing technique and were further verified by quantitative reverse transcriptase polymerase chain reaction (qRT PCR) assay. Lung damage is mainly with characteristics of lung interstitial fibrosis, upregulation of rno-miR-212, rno-miR-144, rno-miR-702-3p, rno-miR-379 and rno-miR-127, down-regulation of rno-miR-541 at 60^{th}, 90^{th} d post-exposure. As target genes of rno-miR-208, rno-miR-212 and rno-miR-18a respectively, there was no statistical significance of programmed cell death 4 (PDCD4), LIN28B and connective tissue growth factor (CTGF) mRNA expression level ($P > 0.05$) compared to β-actin as internal controls detected by Real-time quantitative PCR. The differences in protein gray value ratio of PDCD4, LIN28B and CTGF detected by Western blotting test were statistically significant ($P < 0.05$). These results suggested that miR-208, miR-212 and miR-18a may take effects in rats' lung damage lead by nanosized SiO_2. Their target genes of PDCD4, LIN28B and CTGF functioned in translation level of target genes in regulation of inflammatory signaling pathways and involved in the formation of tissue fibrosis.

ARTICLE HISTORY
Received 13 July 2016
Revised 5 August 2016
Accepted 8 September 2016

KEYWORDS
miRNAs expression profiles; nanosized SiO_2; pulmonary injury; target genes

Introduction

Microsized SiO_2 represented by quartz is a typical pulmonarytoxicant to cause silicosis.[1] It was determined as class I carcinogen by IARC in 1997 as its carcinogenic effects on sufficient evidence in animals and epidemiological investigation. Nanosized SiO_2 has the same chemical composition as microsized SiO_2 and is widely used in almost all areas involved in the microsized SiO_2 powders.[2,3] It is particularly important to research its biological safety. Now it did not have the unified, clear conclusions for the pulmonary toxicity of nanosized SiO_2. Some studies have reported that obvious pulmonary inflammation reaction and pathology change were not observed after mice or rats exposure to nanosized SiO_2.[4-6] However, some studies drew diametrically opposite conclusions from their experiences. Nanosized colloid SiO_2 possess greater capacity to give rise to pulmonary inflammatory reaction and tissue injury than microsized colloid SiO_2 because of bronchiolar epithelial cells in nanosized colloid SiO_2-treated mice showing more severe vacuolation and necrosis in comparison with microsized colloid SiO_2-administrated mice at 12 and 24 h post-exposure by intratracheal instillation.[7] Ultrafine amorphous silica could induce intense alveolar epithelial thickening and lung fibration at 1 week.[8] Lesion characteristics in lung tissue of rat after intratracheal instillation nanosized SiO_2 are alveolar collapse, inflammatory reaction, granuloma formation, alveolar septum thickening and bronchiolar epithelial shedding.[9] In recent years, microRNA (miRNA) as a small non-coding RNA to regulate extensive genes attracted the attention of the scientific community. It supplies a new means for the study on molecular mechanism of lung damage evolution caused by nanosized SiO_2 in view its regulating action of and playing a vital role in the expression of genes associated with organs fibrosis. Studies have found that miR-16 and miR-127 may take part in the process of acute pulmonary injury of mouse induced by lipopolysaccharide.[10,11] It was

CONTACT Hong Yang yanghongr@seu.edu.cn Key Laboratory of Environmental Medicine and Engineering, Ministry of Education, School of Public Health, Southeast University, Nanjing, P.R. China.

Color versions of one or more of the figures in this article can be found online at www.tandfonline.com/kbie.

found that miR-21 and miR-29 families play an important role in the pulmonary fibrosis model of mice induced by bleomycin.[12,13] The miRNA target genes analysis showed the let-7f may participate in the mainly related gene expression in advanced fibrosis signaling pathways of pulmonary injury induced by bleomycin.[14] The miR-126 expression decreased in lung epithelial cells of cystic fibrosis patients, at the same time, miR-126 can adjust TOM1 gene expression of TLR 2/4 signaling pathways.[15,16] The studies suggest the miRNA can regulate pulmonary injury process through various approach. The study of differentially expressed microRNAs in pulmonary injury induced by nanosized SiO_2 is conduciveto further understand of the development mechanism of pulmonary injury and look for molecular control targets.

On the basis of our previous studies, rats' pulmonary injury model with intratracheal instillation of nanosized SiO_2 was established.[17] Illumina HiSeq2000 was used to analyze miRNAs expression profiles in pulmonary tissue of rats different doses, time exposed to nanosized SiO_2 with reference to normal, then to find specific miRNAs expression and predict their target genes, and to investigate the biological function and regulation effect of miRNA in the lung lesion process caused by nanosized SiO_2. It provided a scientific basis to reveal the molecular mechanisms and biomarkers of pulmonary toxicity induced by nanosized SiO_2.

Materials and methods

Animal experiment

All animal experiments were performed in compliance with the local ethics committee. Specific pathogen-free male healthy Sprague Dawley rats, weighted 180–220 g and at 7 weeks of age were purchased from Shanghai Laboratory Animal Research Center (Shanghai, China) and acclimatized for 3 days, then each rat was inspected to verify fit for experiment. Rats were bred in single cages and had free gain to food and water. The animals were housed in in an animal facility under temperature of 25 ± 1°C, relative humidity of 45 ± 5%, and 12 h light/dark circle. 150 rats were separated into 5 groups in a random order. They were instilled intratracheally with 1 mL suspension of saline, 6.25, 12.5, 25 mg/mL nanosized SiO_2 and 25 mg/mL microsized SiO_2 particles and were sacrificed at the 7^{th}, 15^{th}, 30^{th}, 60^{th} and 90^{th} d post-exposure from each group with 6 rats. Nanosized SiO_2 was provided by Zhejiang Hongsheng Material Technology Co., Ltd. (Zhejiang, China). The SiO_2 and the hydroxy group content of the nanosized SiO_2 was greater than 99.5% and 45% respectively. The surface area of the nanosized SiO_2 was 640 ± 50 m^2/g (as provided by the production company). The microsized SiO_2 powder was obtained from Sigma-Aldrich (cat. no. 5631, USA), in which approximately 80% of the SiO_2 particles were between 1–5 μm in diameter, and the purity was 99% according to safety data sheet. Particles size of nanosized SiO_2 and microsized SiO_2 particles suspended in physiological saline determined by Malvern Lazer Particle Analyzer (Fig. 1).The suspensions were dispersed by ultrasonic vibration for 15 min before intratracheal instillation.

Sample collection and RNA extraction

Rats in each group were killed with 0.1 ml pentobarbital sodium solution injected intraperitoneally at the 7^{th}, 15^{th}, 30^{th}, 60^{th} and 90^{th} d after instillation. Lung tissues were removed from chest and immediately put in liquid nitrogen to frozen. Total RNA in rats' pulmonary tissue from each group was extracted with TRIzol®Regent (Invitrogen, USA) in accordance with supplier manual. The quality and quantity of the total RNA were detected with Nanodrop2000 Micro-spectrophotometer (Thermo Scientific, USA). RNA integrity in each sample was determined by agarose gel electrophoresis.

miRNA sequence analysis

15% denaturing polyacrylamide gel electrophoresis was applied to separate 16–30 n small RNAs from the total RNA samples by size fractionation. Proprietary adaptors (Illumina, USA) were then bind to the 5′ and 3′ ends of the small RNAs and reversed transcription was carried out in accordance with the protocol. Small cDNA libraries were augmented by PCR applying primers complementary to the adaptor sequences. The cDNA libraries were then deep sequenced using the HiSeq2000 system (Illumina, USA) at Biorefer (Shanghai, China), in the light of manufacturer's directions.

As an initial filtering step, unqualified reads, 3′adaptor reads, reads with 5′ adaptor contaminants and reads shorter than 15nt were eliminated. The spare sequences were matched to the Rattusnorvegicus

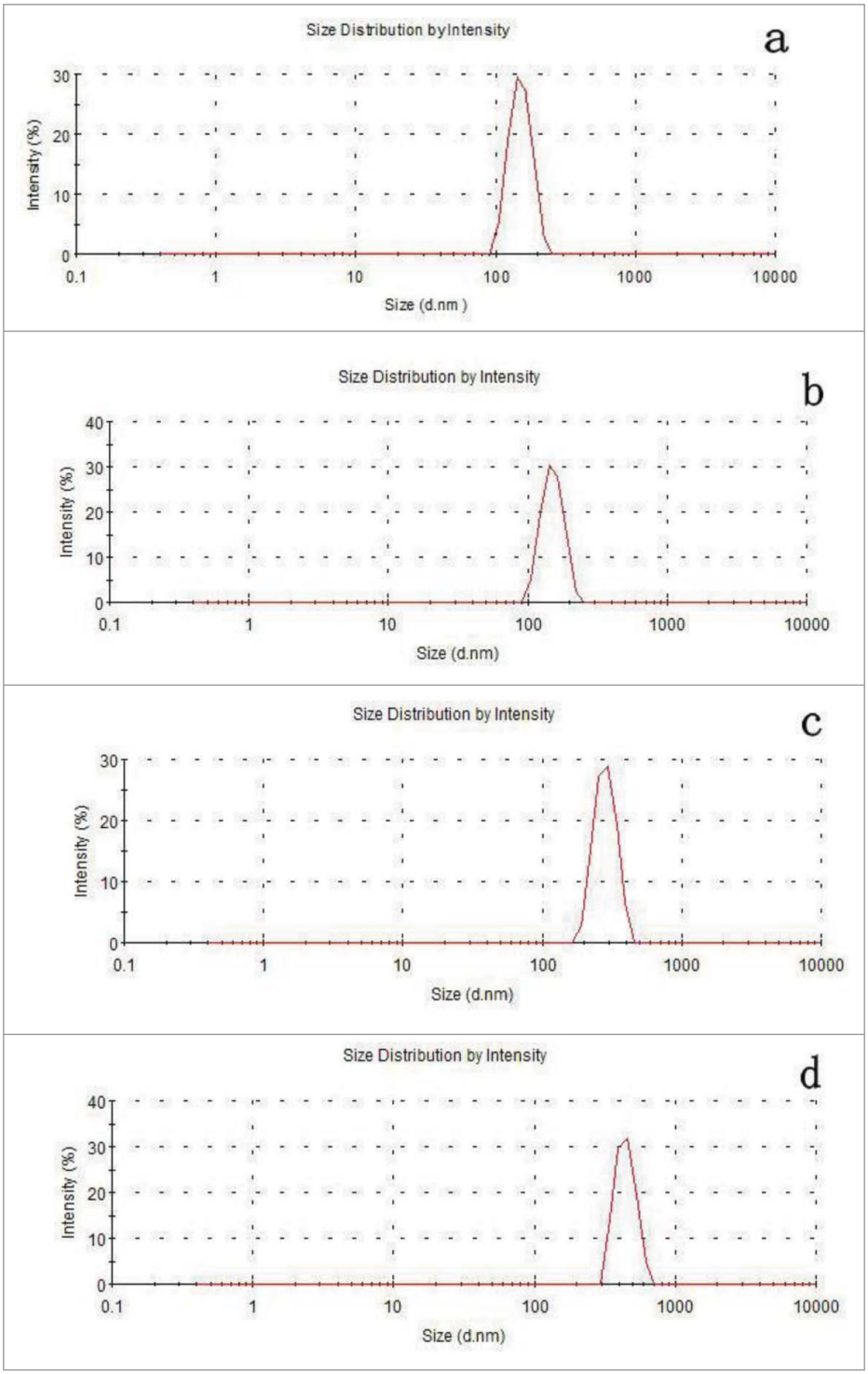

Figure 1. Illustrations of particles size of nanosized SiO_2 and microsized SiO_2 particles suspended in physiological saline determined by Malvern Lazer Particle Analyzer. (A) 6.25 mg/mL nanosized SiO_2; (B) 12.5 mg/mL nanosized SiO_2; (C) 25 mg/mL nanosized SiO_2; (D) 25 mg/mL microsized SiO_2 particles.

(Norway rat) genome applying the BWA procedure with a common difference of 2 mismatched. The mapped sequences were compared with the miRBase data base (http://www.mirbase.org/) to distinguish percolating through rRNAs, tRNAs, snRNAs and snoRNAs. On the basis of sequence similarity, the spare reads were divided into different categories and aligned to the miRBase version 20.0 database (http://www.mirbase.org/) to recognize conservative miRNAs. According to research needs, a target molecule

expression pattern analysis was selected. Known miRNA expression profiles were obtained by DESeq. MiRNA expression levels were estimated by base mean value, and the normalization process realized by software. The fold change of miRNA expression levels between the test and control groups was calculated by the formula: fold change = log 2 (test/control).

Real-time quantitative PCR analysis

Specific miRNA primers and the Reverse Transcription System (Promega, USA) were used for reverse-transcription of miRNAs. Each 20 μL reaction volume in PCR tube was consisted of 4 μL of $MgCl_2$, 2 μL of reverse-transcription 10 × Buffer, 2 μL of dNTP Mixture, 0.5 μL of Ribonuclease Inhibitor, 0.6 μL of AMV Reverse-transcriptase, 6.9 μL of RNase free H_2O, 2 μL of extracted RNA sample, and 2 μL of primer. Reverse-transcription was conducted utilizing PCR system (Promega, USA) as the following conditions: incubated reactions at 42°C for 15 min, 95°C for 5 min, and then 4°C for 5 min. Amplification of real-time PCR was carried out using the Go Taq®qPCR Master Mix (Promega, USA). Each 20 μL reaction volue in in PCR tube contained 4 μL of cDNA sample, 10 μL of 2 × GoTaq®qPCR Master Mix, 0.8 μL of miRNA specific forward primer (5 μM), 0.8 μL of universal reverse primer (5 μM), 0.2 μL of CXR Reference Dye, and 4.2 μL of RNase free H_2O. Thermocycling was conducted appling Real-Time PCR System (Applied Biosystems, USA) as follows: original denaturation of 95°C for 2 min, next by 40 cycles of denaturation at 95°C for 15 s, annealing at 60°C for 60s. Subsequently, melting curve procedure was carried out. U6 small nuclear RNA (U6 snRNA) was use as the internal reference. The result was calculated via the CT method [$\triangle CT = CT_{miRNA} - CT_{U6\ snRNA}$] normalized with respective internal controls. β-actin was used as the internal reference for mRNA determination of PDCD4, LIN28B and CTGF utilizing Reverse Transcription System and GoTaq®qPCR Master Mix (Promega, USA). Real-time PCR protocol was initiated at 95°C for 2 min, following by 40 cycles adopting amplification parameters of denaturalizing at 95°C for 15 s and annealing at 60°C for 60 s in accordance with the primer (as shown in Table 1) set used. After the end of amplification cycle, melting curves were systematically measured. The data was calculated via the CT method [$\triangle\triangle CT = CT_{mRNA} - CT_{\beta\text{-actin}}$].

Table 1. The primer of sequences amplifying gene for PCR detection.

Gene	Primer sequence (5′-3′)
PDCD4	Forward:GGATGAGACGGCGTTTGAGAAG
	Reverse: CTAAGGACACTGCCAACACGGG
LIN28B	Forward:GAGGGGCAGGAGAGGTAACAAA
	Reverse: GGTACAGTAGAGGCAAGTGAAGCG
CTGF	Forward:AGCCAGGGAGTAAGGGACACGA
	Reverse: CCACAGCAGTTAGGAACCCAGATT
β-actin	Forward:CTGAACCCTAAGGCCAACCG
	Reverse: GACCAGAGGCATACAGGGACAA

The gene primers applied for PCR were planned by Shanghai Generay Biotech Co.,Ltd, and liquefied in free RNase H_2O and conserved at −20°C.

Target gene prediction and analysis of differentially expressed miRNA

Target gene of respective differentially expressed miRNA was confirmed applying the TargetScan (http://www.targetscan.org/) divination packages. Functions categories of predicted target genes significantly related to miRNAs were ascertained by a GO (http://www.geneontology.org) biological process analysis and a Kyoto Encyclopedia of Genes and Genomes KEGG pathway analysis (http://www.genome.jp/kegg/pathway.html).

Protein dissociation and western blotting

The protein expression level of PDCD4, LIN28B, CTGF and β-actin regarded as the internal reference was detected by western blotting. 30 mg lung tissue was grinded in 400 μL RIPA lysis buffer (Promega, USA) with 4 μL PMSF for tissular protein extract. The concentration of tissular protein was measured using Pierce® BCA Protein Assay Kit according to instruction. 10 μg proteins were electrophoresed on 10% SDS-PAGE.

Then these separated proteins were transferred to a PVDF membrane. In succession, the membrane was blocked by means of incubation in 5% nonfat dry milk at 25°C for 2 h. Incubation with primary monoclonal antibodies (as shown in Table 2) diluted in 5% filtered nonfat dry milk was conducted to overnight at 4°C after cleaning 3 times for 5 min at 25°C applying 1 × TBST buffer. Following washing 3 times again with TBST for 10 min, PVDF membrane was incubated with goat antirabbit IgG antibody (1:10000) combined with 5% horseradish peroxidase (HRP) solution for 1h at 25°C. Results were mensurated utilizing strengthened ECL chemilluminescence and

Table 2. Main antibodies applied for Western blotting detection.

Proteins	Antibodies	Company	Antibody concentration
PDCD4	rabbit antibody PDCD4	CST, USA	1:1000
LIN28B	rabbit antibody LIN28B	CST, USA	1:1000
CTGF	rabbit antibody CTGF	Abcam, England	1:1000
β-actin	rabbit antibody BETA-ACTIN	CST, USA	1:1000

analyzed with the help of an automatic digital gel image analysis system (Tanon-5500, Shanghai, China).

Results and discussion

Small RNA profiles in test and control groups

In order to confirm miRNAs concerned with rats' pulmonary damage caused by nanosized SiO_2, self-reliant pulmonary small RNA libraries were created from the test and control groups and then sequenced applying the Illumina HiSeq2000 platform. After removing inappropriate sequences on the basis of screening matched conditions, the number of raw reads produced from the test and control libraries and be mapable to the reference genome were seen in Table 3. The majority of small RNAs were 21–23nt in length with similar dimension distributions of the reads in the 2 libraries. The above findings reveal that rat pulmonary comprise an enormous amount of multifarious categories small non-coding RNAs as same as other tissues. They may be conducive to the regulatory effect of gene expression during tissular damage.

Identification of conserved rat miRNAs were carried out by miRNAs sequences in the libraries derived from the test and control groups contrasted with those of the 449 precursor miRNAs and 728 mature miRNAs from Rattusnorvegicus cataloged in miRBase version 20.0. 452 mature miRNAs were gained from 2 libraries in dividing into group and matching uniform sequences afterward. By compared with the control group, the number of miRNA up-regulated expression was 395, 314, 278, 241, and down-regulated expression was 127, 167, 135, 412 in 6.25, 12.5, 25 mg/mL nanosized SiO_2 and 25 mg/ml microscale SiO_2 group, respectively (Fig. 2). The common differentially expressed miRNAs of pulmonary injury in an early stage (7^{th}, 15^{th}, 30^{th} d) caused by nanosized SiO_2 was rno-miR-208 and rno-miR-212 upregulated respectively, and the common differentially expressed miRNA of pulmonary injury in later stage (60^{th}, 90^{th} d) was rno-miR-18a up-regulated.

Previous studies have demonstrated RvD1 upregulated miR-21, miR-146b, and miR-219 and downregulated miR-208a in self-limited murine peritonitis at 12 h.[18] Other studies suggested that miR-208 is related to heart disease.[19-21] It played a role in cardiac fibrosis.At present the study of miR-212 mainly focus on the regulation effects of cancer,[22-25] it belongs to a member of the family of miR-132. Previous studies pointed out that some of the target genes of miR-132 mediated neural development, synaptic transmission, inflammation and angiogenesis. MiR-18a highly expressed in lung cancer cells,[26] and it can participate in heart failure related to age through regulating the expression of CTGF. Our research showed that rno-miR-208, rno-miR-212 and rno-miR-18a were in different expression. Further researches are needed to explore whether rno-miR-208, rno-miR-212 and rno-miR-18a participate in rats' lung damage process caused by nanosized SiO_2.

qRT-PCR validation and miRNA target prediction

The differential expression levels of rno-miR-208, rno-miR-212, rno-miR-18a were detected and validated in the test and control samples utilizing real time quantitative RT-PCR (qRT-PCR). The results verified that the expression levels of rno-miR-208, rno-miR-212, rno-miR-18a in the test group were significantly higher than those in the control group (Table 4). qRT-PCR analysis was in accordance with highthroughput sequencing. It indicated that the number of reads

Table 3. Summary of trimmed mapping reads generated from the test and control libraries.

Groups	Concentration(mg/mL)	7^{th} day	15^{th} day	30^{th} day	60^{th} day	90^{th} day
saline	0	23747572	—	—	—	16925541
nanosized SiO_2	6.25	19803085	19733701	26277385	20956898	20316290
	12.5	20190251	17314778	19958679	20400638	19212543
	25	18047908	24090566	20679360	21752819	24750540
microsized SiO_2	25	22684369	17692063	21776384	19855398	17944646

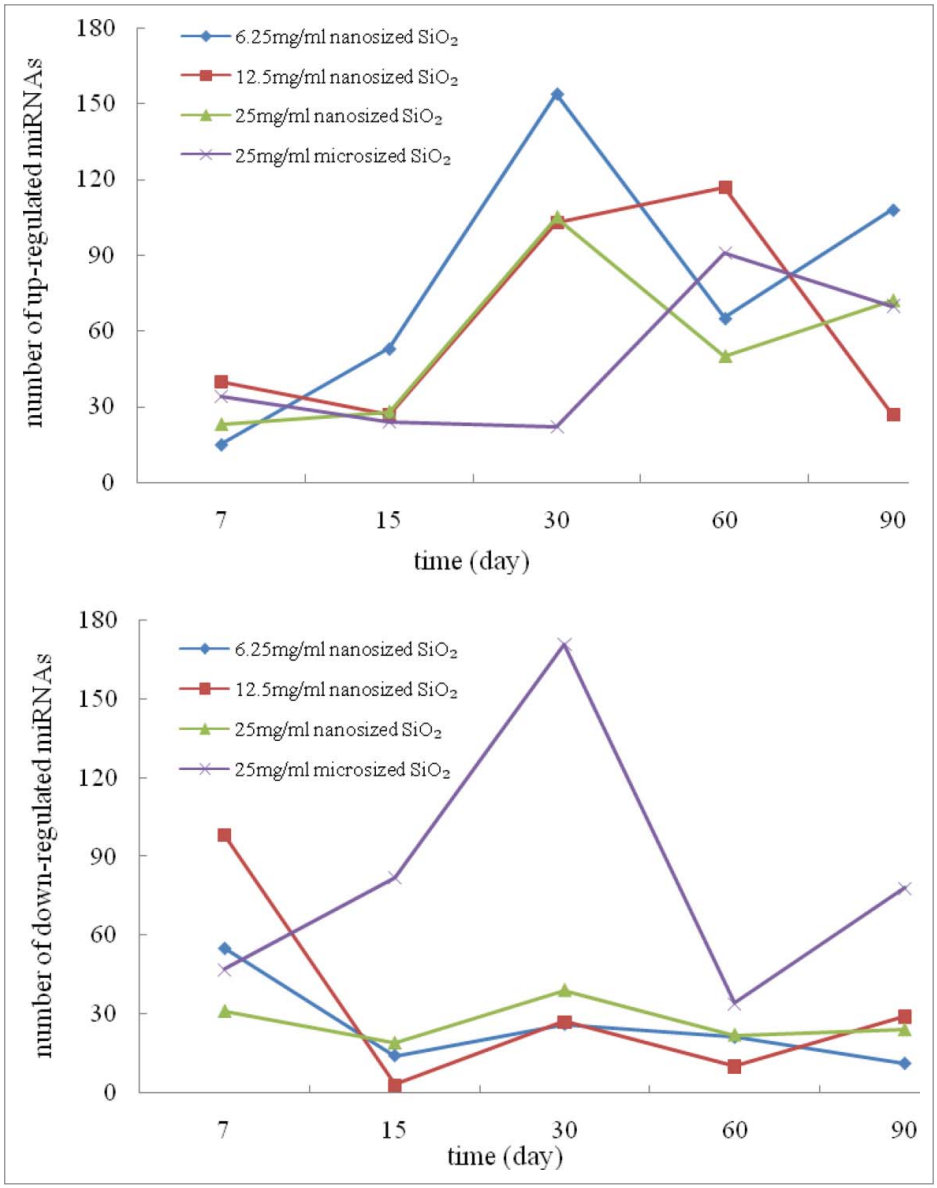

Figure 2. Number of miRNAs upregulated and down-regulated.

derived from highthroughput sequencing is credible for quantifying miRNA expression. Next, illative targets of above miRNAs were forecasted by Targetscan software according to homologous sequences in the Rattusnorvegicus genome. The predictive results showed that the amount of target genes of rno-miR-208, rno-miR-212, rno-miR-18a were 146, 310 and 184 respectively (Table 5). Results of Go and pathway analysis showed that rno-miR-208 mainly involved in the development of lung, lung morphogenesis and lung formation, the signaling pathwaysmainly included T cell receptors signaling pathways, B cell receptor signaling pathways. rno-miR-212 mainly involved in lung development, interstitial development, MAPK cascade regulation, insulin growth factor receptor signaling pathways and epidermal growth factor receptor signaling pathways, the signaling pathways mainly included the MAPK signaling pathways, chemokine signaling pathways, TGF-β signaling pathways.rno-miR-18a mainly involvedin lung development, development of connective tissue, TGF-β stimulus response, the signaling pathways

Table 4. Relative expression level of rno-miR-208, rno-miR-212andrno-miR-18a between test and control groups.

microRNA	$2^{-\Delta\Delta Ct}$	*P* value
rno-miR-208	2.683 ± 0.54	<0.05
rno-miR-212	16.49 ± 2.63	<0.05
rno-miR-18a	1.684 ± 0.16	<0.05

Table 5. Target genes of rno-miR-208, rno-miR-212 and rno-miR-18a.

miRNA	Predicted target genes
rno-miR-208	PDCD4, DDX5, VAV3, CHD9, ETS1, CSNK2A2, MED13, MTF2, CBX1, CDK14, NLK, RAB11A, LRRTM1, ERRFI1, FLJ36031, SOS2, PTPDC1, PIM1, TMBIM6, H2AFY, GPBP1, REEP1, ARGLU1, SECISBP2L, SOX6, FNIP1, SHISA6, RNF145, PTAR1, APC, HNRNPC, SOX5, PGAP1, RAB5C, NAV2, SLC35A4, PHF21B, RANBP9, CDKN1A, EDAR, PURB, UTP18, LCOR, VCPIP1, RFX7, CDCA4, KIAA2018, LRP6, EIF4G2, C1orf151, KCNN3, DPYSL2, GLYR1, PTPRG, HP1BP3, MTMR3, MYCBP, GABRA1, FNIP2, RHOBTB3, ILF3, SNRK, PPP3CB, FAM110B, EYA4, OSBP, POGZ, ASB7, CSNK1D, EIF5, GATA4, EIF4E3, TESK2, ZNF24, FZD8, PACS2, EEF1A1, SCN2B, DDX3X, FNDC3A, LRRC8A, COLQ, HIC2, EEA1, SCRN1, ARID2, CDH2, AMOT, PTBP2, CCRN4L, LRCH2, USP53, ANKRD40, BHLHE41, NRIP1, ZSWIM6, DYNLT1, SLAIN2, KIAA0141, RIMS1, MYEF2, EBF1, COL4A3, CELSR1, SATB1, MYH10, KPNA3, ANKRD13C, TCF12, SP3, TBC1D22B, EDNRB, UBN2, LETMD1, IRS2, TSPAN12, SH3BGRL3, CMIP, EFNB1, ZEB2, IKZF2, USP24, EFHA2, FOXP2, NOVA1, EML4, QKI, NR2C2, ARID5B, TSHZ2, CDC27, CSNK1G1, MAP3K2, ZMYM2, GXYLT1, CLYBL, FZD4, SRCIN1, FEM1C, SLC24A2, KCNQ5, BCL11B, MEIS1, DYRK2, RAB8B, KLHDC5
rno-miR-212	LIN28B, NACC2, SOX5, HMGA2, ZFYVE1, FOXP2, CALU, DYRK2, SGK3, C8orf44-SGK3, NCALD, EP300, BRWD1, SLC6A1, CBLL1, TBC1D30, TIMM9, DPYSL3, RRAS2, LRRFIP1, MEX3C, NOVA1, USP9Y, USP9X, PDE7A, C14orf43, BOLL, UBE2D2, LEMD3CHSY1, TJAP1, MYCBP2, ADAMTS6, ACVR2B, FAM91A1, ELF2, ITCH, PAIP2, SEMA4G, CACNG2, PHF20L1, SAMD12, MED28, DUSP9, SEMA6A, PRICKLE2, E2F5, LSM11, SREBF1, CCDC117, CLASP2, DNAJA2, BRCA1, SLC13A3, SNX29, FOXA1, CSDE1, ARHGEF11, MAPKAP1, SALL1, FLJ36031, C19orf47, KLHL11, ZNF238, PPFIBP1, SLC30A6, DAZAP2, SPPL3, H2AFZ, ARHGAP32, ZCCHC11, TLN2, TSPYL5, OSBPL8, ANP32A, CBFA2T2, HBGF, SLTM, CDC40, TMEM151B, GB1, PAPOLA, SSH2, SRSF1, KCNJ18, C5orf13, GPD2, SPRY1, LARGE, RGS7BP, BNC2, PCDH10, TSPAN18, PCGF3, BCAN, FAM167A, C11orf9, DCC, ETD5, ETV1, SV2A, GLCCI1, NRCAM, SCN1A, COL5A2, ISL1, GALNT13, FKBP2, CLMN, KIF21B, FBXO21, DCUN1D3, FXR1, FOXO3, KCNJ12, KCNA6, ADCY3, ITPKB, CREB5, RASA1, SCN3A, PALM2, TCF15, CFL2, TADA2B, ARHGEF9, HMGXB4, SCN2A, PTBP2, CPSF6, SALL3, BMP3, MAPKBP1, C14orf147, RFX3, ZFC3H1, ProSAPiP1, CHRNA5, TUSC2, EIF5A2, NMNAT2, KBTBD13, GTDC1, SLC5A12, TCF7L1, CDC42BPA, HNRNPU, MAPT, TLK2, SLC2A1, POM121, POM121C, TMED7, KDM5B, HIP1R, NR4A2, STX16, SOS1, H3F3B, ARID2, VAPA, SAP30L, ABCG4, ARID1B, FEM1C, SLC6A3, TAF4B, SLC31A1, BTBD7, TCEB1, FAT2, ASB1, PPP2R5C, ARIH1, NRG2, FBXL20, C21orf91, ZSWIM6, CDKN1A, SEC16A, SPIN1, NFYA, MLLT6, NTNG1, GATA2, HN1, RAB15, RSU1, ARFGEF2, EIF4A2, CHST11, LIMD2, ZNF609, KDM5A, HIC2, CDK19, ETNK1, ARX, RAB6B, ZNF395, PSMA2, NFIB, KIAA0240, CRAMP1L, HIVEP1, HAO1, MEPCE, ZNF292, TSC22D3, FOXN3, KCNK2, ARHGEF40, GPR137C, DOK4, BNIP2, TMEM2, ATXN1, MAPK1, TCF7L2, BTG2, PRR14L, SMARCA5, MAP3K3, IMMP2L, SEC62M, ECOM, PAX7, ENAH, ZNF704, GMFB, DYNLL2, KIAA1211, ANKS1A, OLFM1, AMD1, PTCH1, SOX4, PRKD1, GNA12, ARHGEF10, ZNF644, TTI1, OTUD7B, C7orf60, MEIS1, SNX30, PRRT2, ZNF516, KSR2, AFF2, TUSC3, NET1, MMP16, PAM, PXN, MAMDC2, CERK, BBX, GIGYF1, TRIB2, PEA15, COLQ, FBXW7, SIX4, FOXP1, FGFR3, DCUN1D4, BMP2, ADAMTS5, TNRC6B, SLC12A6, SNX18, RASSF3, CTDSPL2, ACTR3B, AEBP2, MEX3A, SPRED1, ZEB2, MECP2, HAPLN1, TNNI1, RUNX1T1, QKI, DCLK1, YWHAG, PDE7B, BAIAP2, LOC100507421, ELFN2, MAF, KCNN3, ABHD5, SOX6, PPPDE1, C18orf25, MIB1, DCAF8, BSN, PHIP, GSK3B, NFAT5, UNKL, CCNT2, FRMPD4, ZFX, RPL13A, KLHDC10, PFN2, ACTB
rno-miR-18a	CTGF, EPB41L1, TMEM170B, AGPAT3, ATXN7L1, ATXN1, UBE2G1, RUNX1, SH3BP4, SLC12A6, MAP7D1, PHF20L1, ZNF367, KLHL20, MYLK, MAP3K1, GPR37, RORA, CDK19, HMBOX1, GIGYF1, TRAPPC10, VMA21, FRYL, ESR1, NCOA1, ZFP62, TSHZ3, XYLT2, FAM136A, INADL, C17orf100, NEDD9, INO80D, RELL2, PSD3, CREBL2, RABGAP1, MAPK4, IRF2, ETV6, SMAP2, PTGFRN, SORBS2, ADD3, TMEM192, SOX6, HIF1A, DUSP16, WBP2, F3, PKNOX1, HSF2, ORAI3, SMAD2, ENC1, FBXO34, LSM14B, ATXN1L, DMXL2, MYO1C, OLFML2B, BRWD3, RAB11FIP2, BTG3, NXT2, SIM2, UBTD2, NOTCH2, OSBP2, KDM5B, C18orf32, PIAS3, C5orf30, FNBP1, ASXL2, GNPDA2, RPL17-C18ORF32, TEX2, ARHGAP5, IGF1, RAB5C, FAM192A, KCNH7, AKR1D1, TRIOBP, PHF19, STK4, BBX, USP24, THRB, FBXL3, CADM2, LAT, C6orf204, SIX3, KIT, ZSCAN30, NR1H2, ODZ3, NFAT5, FCHSD2, NRG1, AEBP2, PTP4A3, POU6F1, NUPL1, BHLHE22, PHF2, FOXH1, PDZD2, MDGA1, MEF2D, MYL6, ZNF704, CLIP3, C1orf9, HCFC2, CAMKK2, CTDSPL, CLCC1, ODZ4, CSRNP3, IGF2BP2, KCNA1, SAR1A, KCTD16, ZBTB4, C7orf42, TRIM2, DIP2C, ZBTB47, CACNB3, NDFIP1, ADAMTS9, TRIB2, DPP10, LIF, ALCAM, RLIM, FRS2, KIAA0907, ZNF207, UBE2Z, KDM2A, DOCK4, EHMT1, CRIM1, SYNCRIP, TRAPPC8, SATB1, ROBO2, C1orf21, SMARCC2, C5orf13, ATP8A1, CCDC88A, SLC1A2, FGFR3, ADAT2, LIN28A, ANKRD50, TNRC6B, FKBP5, KLHL15, UHMK1, NR3C1, POU2F1, SH3PXD2B, GDAP2, ZNF618, HIPK2, LPP, NAA50, NUFIP2, ZBTB44, ZNF275, MTF1, ANKRD52, NAV1, C14orf43, IGSF3, HMG20B, CSDA

mainly included the MAPK signaling pathways, endocytosis and cancer.

Target genes and proteins expression in test and control groups

Target gene analysis and literature reports showed that rno-miR-208 and rno-miR-212 respectively functioned through their target genes PDCD4, LIN28B to participate in the regulation of inflammatory signaling pathways. rno-miR-18a functioned through its target genes CTGF involved in the formation of tissue fibrosis. Real-time quantitative PCR and Western blotting test were detected the level of PDCD4, LIN28B mRNA and proteins at 7^{th} d post-exposure to nanosized SiO_2, CTGF mRNA and proteins at 60^{th} d post-exposure to nanosized SiO_2 in rat pulmonary tissue compared to normal saline group. The results showed the expression level of PDCD4, LIN28B mRNA were 1.02 ± 0.02 and 1.04 ± 0.05 with no statistical significance of differences ($P > 0.05$) in comparison with β-actin internal controls, the protein gray value ratio were 0.27 ± 0.02, 1.14 ± 0.15 and 1.19 ± 0.12, 0.23 ± 0.04. There were statistical significance of differences ($P < 0.05$) (Fig. 3A, 3B). The level of CTGF mRNA expression was 1.97 ± 0.06 with no statistical significance of differences ($P > 0.05$) in comparison with β-actin internal controls. The protein gray value ratio were 1.04 ± 0.12 and 0.06 ± 0.01, There was statistical significance of difference ($P < 0.05$) (Fig. 3C).

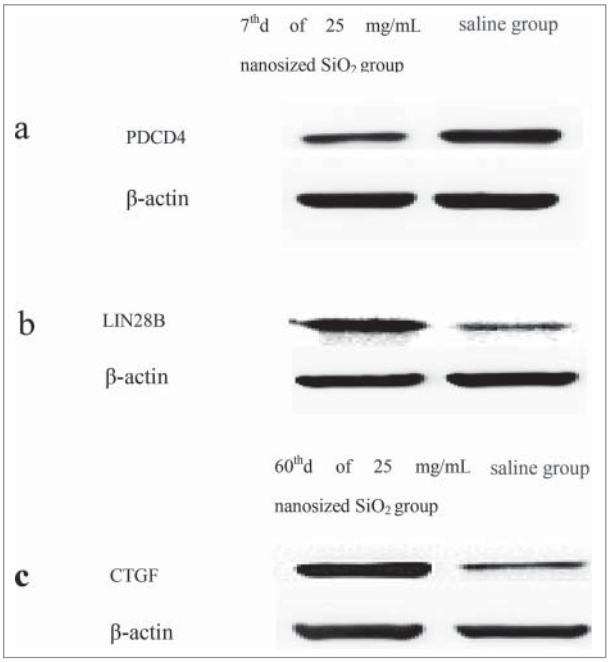

Figure 3. Western blotting of PDCD4, LIN28B and CTGF. (A) PDCD4; (B) LIN28B; (C) CTGF.

Early studies have illustrated that PDCD4 take an important effect in inhibiting tumor development. However, in recent years, studies found that PDCD4 also play an important role in some inflammatory disease. Study on mechanism stated clearly that activated PDCD4-devoid lymphocytes preferentially engendered cytokines promoting oncogene rather than inhibiting inflammation. PDCD4 dominates lymphoma occurrence and autoimmune inflammatory reaction via alternatively restraining protein.[27] PDCD4 as a tumor-suppressing gene is a pro-inflammatory protein to furtherance activation of the transcription factor NF-κB and inhibit interleukin-10 (IL-10) translation in the immunologic system.[28] Rapamycin improves the TNF-α-induced exudation of IL-6 and IL-8 by inhibiting PDCD4 degradation in orbital desmocytes.[29] These results suggest that PDCD4 functions as pro-inflammatory factor. PDCD4 suppresses the induction of inflammatory mediators of TNF-α and IL-10.[30,31] Inflammatory environment in vivo can induce downregulation of PDCD4 proteins. These results suggest PDCD4 is likely to be an anti-inflammatory factor. LIN28 and LIN28B are homologous genes of LIN28 in mammals, and their functions are similar. Src activation initiates an inflammatory reaction induced by NF-κB that immediately fires LIN28 transcription and expeditiously decreases microRNA levels of let-7. Let-7 straight suppress IL6 expression, leading to higher levels of IL6 than acquired by NF-κB activation. It is necessary for transformation that IL6 activate STAT3 transcription factor, and IL6 activates NF-κB, thereby finishing a positive tickling circle.[32] CTGF was discovered as a kind of important promoting fibrosis cell factor in recent years. It can not only directly stimulate fibroblast proliferation and increased extracellular matrix synthesis, but also mediate the fibrosis induced by TGF-β. Study found that expression of CTGF mRNA and protein levels in pulmonary tissue of patients suffering from idiopathic pulmonary fibrosis were significantly up-regulated. Although individual expression of CTGF in lung tissue induced only mild fibrosis,[33] inhibiting the expression of CTGF can prevent fibrosis formation.[34] microRNA has a lot of different target genes. In the same way, the same target genes often jointly regulated by many different miRNAs. One-to-one relationship between PDCD4, LIN28B, CTGF and target gene of rno-miR-208, rno-miR-212 and rno-miR-18a respectively still needs further validation.

Conclusions

In conclusion this study first described the miRNA expression profile of rats' pulmonary injury induced by nanosized SiO_2. The common differentially expressed microRNAs of pulmonary injury in an early stage caused by nanosized SiO_2 was miR-208 and miR-212 respectively, and in later stage was miR-18a. Target genes prediction and KEGG pathways conducted suggested that the differentially expressed miRNAs regulate pulmonary hypoplasia, signal pathways of MAPK and TGF-β. Their target genes of PDCD4, LIN28B and CTGF functioned in translation level of target genes in regulation of rats'pulmonary injury induced by nanosized SiO_2. It is necessary that additional *in vitro* investigation is carried out to obtain an entire understanding of the connection between miRNA profiles, target genes, and the pathogenesis of rats' pulmonary injury induced by nanosized SiO_2.

Disclosure of potential conflicts of interest

No potential conflicts of interest were disclosed.

Acknowledgments

We thank Nanjing Decode Genomics Biotechnology CO., LTD for assistance with the bioinformatics analysis.

Funding

Research supported by National Natural Science Foundation of China (Grant No.81273046), Preventive Medicine Research Projects of Jiangsu Province (Grant No.Y2012039), and the Fundamental Research Funds for the Central Universities.

References

[1] Davda J, Labhasetwar V. Characterization of nanoparticle uptake by endothelial cells. Int J Pharmaceut 2002; 233:51-9; http://dx.doi.org/10.1016/S0378-5173(01)00923-1

[2] Suriyaprabha R, Karunakaran G, Kavitha K, Yuvakkumar R, Rajendran V, Kannan N. Application of silica nanoparticles in maize to enhance fungal resistance. IET Nanobiotechnol 2014; 8:133-7; PMID:25082220; http://dx.doi.org/10.1049/iet-nbt.2013.0004

[3] Shadjou N, Hasanzadeh M. Silica-based mesoporous nanomaterials as promoter of bone regeneration process. J Biomed Mater Res A 2015; 103:3703-16; PMID:26011776; http://dx.doi.org/10.1002/jbm.a.35504

[4] Sayes CM, Beed KL, Glover KP, Swain KA, Ostraat ML, Donner EM, Warheit DB. Changing the dose metric for inhalation toxicity studies: short-term study in rats with engineered aerosolized amorphous silica nanoparticles. Inhal Toxicol 2010; 22:348-54; PMID:20001567; http://dx.doi.org/10.3109/08958370903359992

[5] He QJ, Zhang ZW, Gao F, Li Y, Shi JL. In vivo biodistribution and urinary excretion of mesoporous silica nanoparticles: effects of particle size and PEGylation. Small 2011; 7:271-80; PMID:21213393; http://dx.doi.org/10.1002/smll.201001459

[6] Guo MC, Xu XL, Yan XC, Wang S, Gao S, Zhu SS. In vivo biodistribution and synergistic toxicity of silica nanoparticles and cadmium chloride in mice. J Hazard Mater 2013; 260:780-8; PMID:23856307; http://dx.doi.org/10.1016/j.jhazmat.2013.06.040

[7] Kaewamatawong T, Kawamura N, Okajima M, Wang S, Shimada A. Acute pulmonary toxicity caused by exposure to colloidal silica: Particle size dependent pathological changes in mice. Toxicol Pathol 2005; 33:745-51; http://dx.doi.org/10.1080/01926230500416302

[8] Choi M, Cho WS, Han BS, Cho M, Kima SY, Yia JY, Ahnb B, Kima SH, Jeong J. Transient pulmonary fibrogenic effect induced by intratracheal instillation of ultrafine amorphous silica in A/J mice. Toxicol Lett 2008; 182:97-101; PMID:18835341; http://dx.doi.org/10.1016/j.toxlet.2008.08.019

[9] Coccini T, Barni S, Vaccarone R, Mustarelli P, Manzo L, Roda E. Pulmonary toxicity of instilled cadmium-doped silica nanoparticles during acute and subacute stages in rats. Histol Histopathol 2013; 28:195-209; PMID:23275303

[10] Cai ZG, Zhang SM, Zhang Y, Mustarelli P, Wu HB, Xu XP. MicroRNAs are dynamically regulated and play an important role in LPS-induced lung injury. Can J Physiol Pharmacol 2012; 90:37-43; PMID:22185353; http://dx.doi.org/10.1139/y11-095

[11] Cushing L, Kuang PP, Qian J, Shao F, Wu JJ, Little F, Thannickal VJ, Cardoso WV, Lü JN. miR-29 is a major regulator of genes associated with pulmonary fibrosis. Am J Respir Cell Mol Biol 2010; 45:287-94; PMID:20971881; http://dx.doi.org/10.1165/rcmb.2010-0323OC

[12] Liu G, Friggeri A, Yang Y, Milosevic J, Ding Q, Thannickal VJ, Kaminski N, Abraham E. miR-21 mediates fibrogenic activation of pulmonary fibroblasts and lung fibrosis. J Exp Med 2010; 207:1589-97; PMID:20643828; http://dx.doi.org/10.1084/jem.20100035

[13] Xie T, Liang JR, Guo RS, Liu N, Noble PW, Jiang D. Comprehensive microRNA analysis in bleomycin-induced pulmonary fibrosis identifies multiple sites of molecular regulation. Physiol Genomics 2011; 43:479-87; PMID:21266501; http://dx.doi.org/10.1152/physiolgenomics.00222.2010

[14] Maltby S, Plank M, Tay HL, Collison A, Foster PS. Targeting microRNA function in respiratory diseases: mini-review. Front Physiol 2016; 7:21; PMID:26869937; http://dx.doi.org/10.3389/fphys.2016.00021

[15] Oglesby IK, Bray IM, Chotirmall SH, Stallings RL, O'Neill SJ, McElvaney NG, Greene CM. miR-126 is down-regulated in cystic fibrosis airway epithelial cells and regulates TOM1 expression. J Immunol 2010; 184:1702-9; PMID:20083669; http://dx.doi.org/10.4049/jimmunol.0902669

[16] Zhang Y, Li W, Zheng Y, Wang X, Li G, Yang H. Dynamic changes of pathological morphology and ultrastructure of lung injury in rats induced by SiO^2 nanoparticles. Zhonghua lao dong wei sheng zhi ye bing za zhi 2014; 32:504-10; PMID:25182818

[17] Recchiuti A, Krishnamoorthy S, Fredman G, Chiang N, Serhan, CN. microRNAs in resolution of acute inflammation: identification of novel resolvin D1-miRNA circuits. FASEB J 2011; 25:544-60; PMID:20956612; http://dx.doi.org/10.1096/fj.10-169599

[18] Oliveira-Carvalho V, Carvalho VO, Bocchi EA. The emerging role of miR-208a in the heart. DNA Cell Biol 2013; 32:8-12; PMID:23121236; http://dx.doi.org/10.1089/dna.2012.1787

[19] Bostjancic E, Zidar N, Stajer D, Glavac D. MicroRNAs miR-1, miR-133a, miR-133b and miR-208 are dysregulated in human myocardial infarction. Cardiology 2010; 115:163-9; PMID:20029200; http://dx.doi.org/10.1159/000268088

[20] Wang BW, Wu GJ, Cheng WP, Shyu KG. microRNA-208a increases myocardial fibrosis via endoglin in volume overloading heart. PloS One 2014; 9:e84188; PMID:24392114; http://dx.doi.org/10.1371/journal.pone.0084188

[21] Zeng J, Fang M, Wang L, Liang X, Shen Y, Yu H, Liu Z, Sun Y, Liu S, Chen C, Jia J. microRNA-212 inhibits proliferation of gastric cancer by directly repressing retinoblastoma binding protein 2. J Cell Biochem 2013; 114:2666-72; PMID:23794145; http://dx.doi.org/10.1002/jcb.24415

[22] Lu L, Zhang XJ, Zhang B, Wu J, Zhang XJ. Synaptic acetylcholinesterase targeted by microRNA-212 functions as a tumor suppressor in non-small cell lung cancer. Int J Biochem Cell Biol 2013; 45:2530-40; PMID:23974008; http://dx.doi.org/10.1016/j.biocel.2013.08.007

[23] Park JK, Henry JC, Jiang J, Esau C, Gusev Y, Lerner MR, Postier RG, Brackett DJ, Schmittgen TD. MiR-132 and miR-212 are increased in pancreatic cancer and target the retinoblastoma tumor suppressor. Biochem Biophys Res Commun 2011; 406:518-23; PMID:21329664; http://dx.doi.org/10.1016/j.bbrc.2011.02.065

[24] Wada R, Akiyama Y, Hashimoto Y, Fukamachi H, Yuasa Y. miR-212 is down regulated and suppresses methyl-CpG-binding protein MeCP2 in human gastric cancer. Int J Cancer 2010; 127:1106-14; PMID:20020497; http://dx.doi.org/10.1002/ijc.25126

[25] Al-Kafaji G, Al-Naieb ZT, Bakhiet M. Increased oncogenic microRNA-18a expression in the peripheral blood of patients with prostate cancer: A potential novel non-invasive biomarker. Oncol Lett 2016; 11:1201-6; PMID:26893719

[26] Hilliard A, Hilliard B, Zheng SJ, Sun H, Miwa T, Song WC, Goeke R, Chen YH. Translational regulation of autoimmune inflammation and lymphoma genesis by programmed cell death 4. J Immunol 2006; 177:8095-102; PMID:17114484; http://dx.doi.org/10.4049/jimmunol.177.11.8095

[27] Sheedy FJ, Palsson-McDermott E, Hennessy EJ, O'Leary JJ, Ruan Q, Johnson DS, Chen Y, O'Neill LA. Negative regulation of TLR4 via targeting of the proinflammatory tumor suppressor PDCD4 by the microRNA miR-21. Nat Immunol 2010; 11:141-7; PMID:19946272; http://dx.doi.org/10.1038/ni.1828

[28] Lee WM, Paik JS, Cho WK, Oh EH, Lee SB, Yang SW. Rapamycin enhances TNF-α-induced secretion of IL-6 and IL-8 through suppressing PDCD4 degradation in orbital fibroblasts. Curr Eye Res 2013; 38:699-706; PMID:23281820; http://dx.doi.org/10.3109/02713683.2012.750368

[29] Yasuda M, Irie K, Murakami A. Inhibition by genistein of the lipopolysaccharide-induced downregulation of programmed cell death 4 in RAW264.7 mouse macrophages. Biosci Biotechnol Biochem 2010; 74:1095-7; PMID:20460704; http://dx.doi.org/10.1271/bbb.90892

[30] Yasuda M, Schmid T, Rubsamen D, Colburn NH, Irie K, Murakami A. Downregulation of programmed cell death 4 by inflammatory conditions contributes to the generation of the tumor promoting microenvironment. Mol-Carcinog 2010; 49:837-48.

[31] Iliopoulos D, Hirsch HA, Struhl K. An epigenetic switch involving NF-kappaB, Lin28, Let-7 microRNA, and IL6 links in ammation to cell transformation. Cell 2009; 139:693-706; PMID:19878981; http://dx.doi.org/10.1016/j.cell.2009.10.014

[32] Bonniaud P, Margetts PJ, Kolb M, Haberberger T, Kelly M, Robertson J, Gauldie J. Adenoviral gene transfer of connective tissue growth factor in the lung induces transient fibrosis. Am J Respir Crit Care Med 2003; 168:770-8; PMID:12816739; http://dx.doi.org/10.1164/rccm.200210-1254OC

[33] Chen YC, Chen BC, Yu CC, Lin SH, Lin CH. miR-19a, -19b, and -26b Mediate CTGF expression and pulmonary fibroblast differentiation. J Cell Physiol 2016; 231 (10):2236-48, Feb 12. [Epub ahead of print]; PMID:26873752; http://dx.doi.org/10.1002/jcp.25341

[34] Ying H, Kang Y, Zhang H, Zhao D, Xia J, Lu Z, Wang H, Xu F, Shi L. MiR-127 modulates macrophage polarization and promotes lung inflammation and injury by activating the JNK pathway. J Immunol 2015; 194:1239-51; PMID:25520401; http://dx.doi.org/10.4049/jimmunol.1402088